COMMUNICATION

Check for updates

Transdermal therapeutic polymer: *in situ* synthesis of biocompatible polymer using 5-aminolevulinic acid as a photosensitizer precursor and a polymer initiator†

Jaehoon Kim,[a] Eun Woo Seo,[b] Hyunyoung Choi,[c] Hyo In Kim,[d] Jinbong Park, [ID][c] Junyang Jung ⋆[abe] and Dokyoung Kim [ID] ⋆[abefghi]

Melanoma is the most malignant skin tumor caused by the malignancy of melanocytes that produce the melanin pigment. Various methods have been developed to combat melanoma, with photodynamic therapy (PDT) gaining the spotlight for its ability to eliminate cancer cells by generating reactive oxygen species through light-sensitive photosensitizers. 5-aminolevulinic acid (5-ALA) is the most commonly used PDT agent, which could be converted to the PpIX photosensitizer molecule within cancer cells. However, its high hydrophilicity limits effective transdermal and oral delivery. In this work, we present a novel polymer formulation, named 5-AP, designed for the transdermal delivery of 5-ALA to deep melanoma tumor sites. 5-AP was prepared by the *in situ* polymerization of dimethylsiloxane, using 5-ALA as a photosensitizer precursor and a ring-opening polymerization initiator. 5-AP exhibited enhanced hydrophobicity compared to 5-ALA, facilitating improved transdermal penetration. In a melanoma mouse model, 5-ALA was released from the polymer and then converted to PpIX, emitting fluorescence and demonstrating high tumor treatment efficacy under laser irradiation. We believe these findings can usher in a new era of transdermal photodynamic therapy.

New concepts

Herein, we present a novel type of transdermal photodynamic therapy agent. We aimed to develop a new polymeric hybrid material (named **5-AP**) based on 5-aminolevulinic acid (5-ALA), the most widely used for photodynamic therapy of cancer in clinical sites. The material was prepared by facile acid-induced one-pot ring-opening polymerization. **5-AP** has dual-functionality as a transdermal drug delivery carrier and photodynamic therapy agent. The low transdermal delivery efficiency of the existing 5-ALA is dramatically improved through dimethylsiloxane conjugation, with a viscosity-suitable enhancement for transdermal treatment. The *in vivo* degradation of **5-AP** released the 5-ALA within the tumor site, and it was confirmed that higher therapeutic efficacy could be induced by the *in situ* generation of the protoporphyrin IX (PpIX) photosensitizer. Since our study is the first report of synthesizing a hybrid material of 5-ALA as a new transdermal photodynamic therapy agent rather than simply loading it, we are confident that it can serve as a pioneer in the development of more diverse types of 5-ALA-based substances and similar new transdermal delivery photodynamic therapeutics.

Introduction

Melanoma is a tumor caused by the malignancy of melanocytes, the cell responsible for producing the melanin pigment.[1–3] Although it can develop in any area where melanocytes exist, melanoma most commonly appears on the skin and is recognized as one of the most aggressive forms of skin cancer.[4] The primary treatment method for melanoma is surgical removal of the lesion.[5,6] However, in the case of metastatic melanoma, chemotherapy is often less effective and can cause serious side effects due to its non-specific drug targeting.[7,8] To address these issues, targeted anticancer drugs such as BRAF and MEK inhibitors have been introduced as new treatment options

[a] *College of Medicine, Kyung Hee University, Seoul 02447, Republic of Korea. E-mail: jjung@khu.ac.kr, dkim@khu.ac.kr*

[b] *Department of Biomedical Science, Graduate School, Kyung Hee University, Seoul 02447, Republic of Korea*

[c] *Department of Science in Korean Medicine, Graduate School, Kyung Hee University, Seoul 02447, Republic of Korea*

[d] *Department of Surgery, Beth Israel Deaconess Medical Center/Harvard Medical School, Boston, Massachusetts, USA*

[e] *Department of Anatomy and Neurobiology, College of Medicine, Kyung Hee University, Seoul 02447, Republic of Korea*

[f] *Department of Precision Medicine, Graduate School, Kyung Hee University, Seoul 02447, Republic of Korea*

[g] *Center for Converging Humanities, Kyung Hee University, Seoul 02447, Republic of Korea*

[h] *KHU-KIST Department of Converging Science and Technology, Kyung Hee University, Seoul 02447, Republic of Korea*

[i] *Medical Research Center for Bioreaction to Reactive Oxygen Species and Biomedical Science Institute, Core Research Institute (CRI), Kyung Hee University, Seoul 02447, Republic of Korea*

† Electronic supplementary information (ESI) available. See DOI: https://doi.org/10.1039/d5mh00099h

for melanoma.[9,10] Despite their advances, these targeted therapies still have limitations due to challenges in individual biochemical and genetic profiling in clinical practice.[11,12] Another melanoma treatment approach is photodynamic therapy (PDT) using a photosensitizer (PS).[13,14] PDT induces cell death by generating reactive oxygen species (ROS) during the process of stabilizing the excited energy of PS when PS absorbs external light.[15,16] However, the efficacy of PDT against melanoma has been limited due to the tumor's melanin pigmentation and the antioxidant defense mechanisms of melanoma cells.[17,18] Nevertheless, PDT remains a promising treatment, particularly for localized cutaneous melanoma, as this skin tumor can be effectively irradiated by light.[19] PDT can precisely control the light exposure site and PS activation as needed, allowing for better selective antitumor activity and fewer side effects compared to conventional radiotherapy and chemotherapy.[20,21]

5-aminolevulinic acid (5-ALA) is the most commonly used PDT agent, which is converted *in situ* into the protoporphyrin IX (PpIX) photosensitizer within cancer cells.[22,23] This conversion allows 5-ALA to selectively target cancer cells without inducing apoptosis in normal cells.[24,25] However, despite its effectiveness as a PDT agent, 5-ALA faces a significant barrier in melanoma treatment due to its high hydrophilicity and polarity, which limits its penetration into the stratum corneum and cell membrane through passive diffusion.[26,27] In this context, the development of a new transdermal drug delivery system (TDDS) utilizing 5-ALA has become essential for effectively treating melanoma.[28] TDDS refers to the delivery of drugs through the skin, offering several advantages over traditional methods such as local or intravenous injection and oral administration.[29,30] Being noninvasive, it reduces pain and improves patient compliance.[31] TDDS also minimizes side effects by bypassing the preferential passage effect of drugs and delivering drugs directly to specific disease sites.[32] Based on these advantages, various methods have been explored using iontophoresis, microneedles, hyaluronic acid, liposomes, ultrasound, and chemical penetration enhancers such as dimethyl sulfoxide and oleic acid to deliver 5-ALA transdermally.[33,34] However, despite these efforts, a newly developed TDDS using 5-ALA still focuses on carriers for substance delivery and often encounters various side effects, such as skin tissue damage and reduced efficacy due to chemical denaturation of the substance itself.[35–37]

Herein, we disclose a novel polymer formulation, 5-ALA-containing polymeric mixture (5-AP), that can transdermally deliver 5-ALA to deep melanoma tumor sites. 5-AP was prepared by the *in situ* polymerization of dimethylsiloxane using 5-ALA as a photosensitizer precursor and a ring-opening polymerization initiator (Fig. 1(a)). Since the siloxane in 5-AP has a strong tendency for lipophilicity, 5-AP has a chemical structure that reduces the high hydrophilicity, which hinders the transdermal delivery of 5-ALA.[38] It also has a viscous formulation suitable for effective transdermal delivery. In addition, as a polymer containing 5-ALA, 5-AP was able to induce the efficacy of 5-ALA. These attributes enable targeted treatment of specific melanoma tumor sites to confirm the successful transdermal delivery of 5-AP (Fig. 1(b)). Upon treatment of 5-AP, 5-ALA was released by the hydrolysis of 5-AP and subsequently converted into PpIX through heme synthesis within the melanoma region, resulting in fluorescence emission. When irradiated with a laser, it demonstrated high efficacy in tumor treatment as a PDT agent. We are confident that 5-AP has the potential to become a
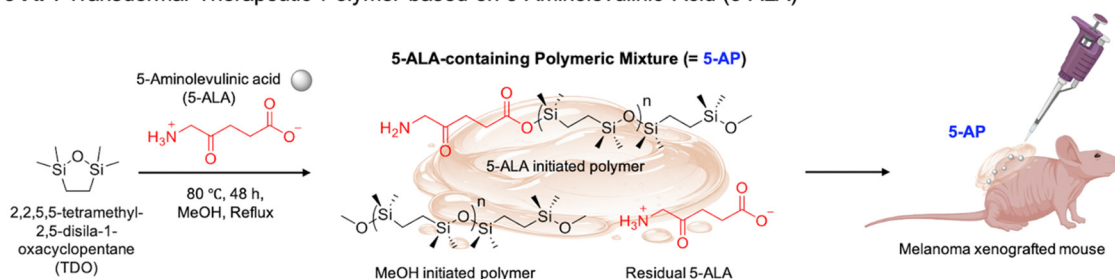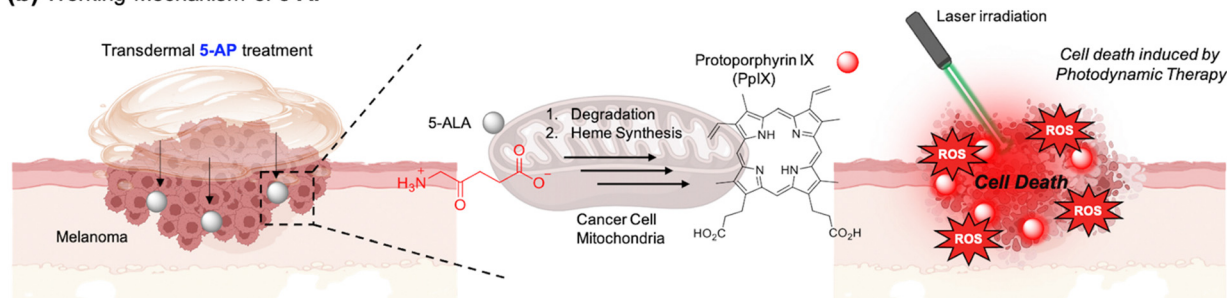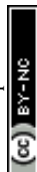

Fig. 1 Research rationale and overview. (a) Schematic illustration of the preparation and application of the material (5-AP). (b) The working mechanism of 5-AP in photodynamic therapy (PDT) for melanoma.

powerful therapeutic candidate for transdermal delivery photodynamic therapy, effectively penetrating the skin and targeting melanoma tumors.

Experimental section

Preparation of 5-AP

2,2,5,5-Tetramethyl-2,5-disila-1-oxacyclopentane (TDOP, 5 mL, 26.66 mmol) was mixed with 5-aminolevulinic acid (5-ALA, 5 mmol) in MeOH (5 mL) and refluxed at 80 °C for 48 h under an argon atmosphere. After the reaction, the resulting product was washed with MeOH (10 mL) three times to remove any unreacted TDOP and 5-ALA. The product was then dried under vacuum to remove the residual MeOH.

NMR analysis of 5-AP

Proton (^{1}H) nuclear magnetic resonance (NMR) spectra were obtained using a JEOL JNM (500 MHz) at 25 °C. Chemical shifts (δ) in the NMR spectra are reported in parts per million (ppm) relative to the signal (0.00 ppm), using tetramethyl silane (TMS) as an internal standard for solutions in CDCl$_3$ (7.26 ppm for ^{1}H). [TDOP]: ^{1}H NMR (500 MHz, CDCl$_3$) δ (ppm): 3.64 (s), 3.42 (s), 1.19 (s), 0.38 (s); [5-AP]: ^{1}H NMR (500 MHz, CDCl$_3$) δ (ppm): 7.25 (s), 0.75 (s), 0.14 (s).

Characterization of 5-AP

To identify the structural changes of 5-AP, gel permeation chromatography (GPC) analysis of TDOP and 5-AP was conducted using high-performance liquid chromatography (HPLC, Agilent 1100 S, Agilent, Santa Clara, CA, USA). The infrared absorption spectra of TDOP, C2, and 5-AP were analyzed using attenuated total reflection Fourier-transform infrared (ATR-FTIR) spectroscopy (Thermo Scientific Nicolet™ iS™ 5 FTIR spectrometer, Waltham, MA, USA). Contact angles of TDOP, C2, and 5-AP were measured using a contact angle meter (DSA100, Kruss, Hamburg, Germany). The viscosity of TDOP, C2, and 5-AP was measured using a rotational rheometer (ARES-G2, TA instrument Ltd, New Castle, DE, USA). The thermal stability of TDOP, C2, and 5-AP was evaluated using thermogravimetric analysis (TGA) (SDT Q600, TA Instruments, DE, USA).

Cell culture

HEK293, b.End3 and B16F10 cell lines were obtained from the Korean Cell Line Bank (Seoul, Rep. of Korea). Cells were cultured in Dulbecco's modified Eagle's media (Hyclone, USA) supplemented with 10% fetal bovine serum (Hyclone, USA) and 1% penicillin–streptomycin (Gibco ThermoFisher Scientific, USA). Cell lines were kept at 37 °C in a humidified 5% CO$_2$ incubator.

Cytotoxicity analysis

The cytotoxicity of TDOP, 5-ALA, and 5-AP was evaluated in the HEK293, b.End3, and B16F10 cell lines using a Cell Counting Kit-8 (CCK-8, Dojindo Molecular Tech. Inc., Japan) according to

the manufacturer's protocols. Cells (5×10^3 cells per well) were seeded into 96-well plates and incubated for 24 h at 37 °C in a humidified 5% CO$_2$ incubator. The medium was then replaced with serum- and antibiotics-free medium to starve the cells and left for 4 h. And then, the cells were treated with diluted concentrations of TDOP, 5-ALA, and 5-AP. After 4 h, the cells were washed twice with Dulbecco's phosphate-buffered saline (DPBS) to remove residual TDOP, 5-ALA, and 5-AP. After that, CCK-8 solution (10 μL, 10% working concentration) in serum-free medium was added to each well of a 96-well plate, and the cells were incubated for 1 h at 37 °C. Absorbance was measured at a wavelength of 450 nm using a microplate reader (Multiskan FC, Thermo Fisher, USA). The percentage of cell cytotoxicity was calculated using the formula; Cell viability (%) = (Mean OD of sample × 100)/(Mean OD of the control group) (OD: optical density). Cytotoxicity results are presented as the mean ± S.E.M. ($n = 3$).

Fluorescence cell imaging

HEK293, b.End3 and B16F10 cells (5×10^3) were seeded onto 35-mm glass-bottom confocal microscopy imaging dishes (SPL, Life Science, Rep. of Korea) and incubated for 24 h. The cells were then treated with 5-ALA and 5-AP and incubated for 24 h at 37 °C in a humidified 5% CO$_2$ incubator. The cells were visualized using a confocal laser scanning microscope (CLSM, Carl-Zeiss LSM 700 Exciter, Germany). Confocal images of 5-ALA and 5-AP (red fluorescence) in all cells were obtained under excitation at 488 nm (laser power: 0.23%) with a detector (GaAsP, detector Gain: 700 V; detection wavelength: 504–700 nm).

Animals

5-Week-old male BALB/c nu/nu mice and BALB/c mice were obtained from DBL Co., Ltd (Incheon, Rep. of Korea). The mice were housed five per cage ($27 \times 22 \times 14$ cm) with free access to food and water in the animal room and were kept under a 12-h light/dark cycle (lights on from 07:30 to19:30) at a constant temperature (23 ± 1 °C) and a relative humidity ($60 \pm 10\%$). The mice were acclimated in the animal room for one week before the start of all experiments. All animal treatments and maintenance were performed in accordance with the Animal Care and Use Guidelines of Kyung Hee University. All experimental protocols were approved by the Institutional Animal Care and Use Committee of Kyung Hee University (Approval No.: KHSASP-23-354). Animal experiments were conducted following international IACUC guidelines. According to guidelines, the maximum tumor size allowed diameter is 20 mm (4160 mm^3, when calculated to volume), and the experiments in this work using tumor xenograft mice were conducted within this range. In addition, no issues with changes in the body weight of mice throughout the experimental period were observed. Given these considerations, there were no ethical issues in the experimental procedures.

Hemolysis assay

Blood samples were obtained from the hearts of the mice anesthetized with isoflurane. Red blood cells (RBCs) were

isolated by centrifugation at 4 °C (2000 rpm, 3 min) and washed twice with cold phosphate-buffered saline (PBS, pH 7.4, 1×). The concentrations of **5-AP** for the test were 125, 250, and 500 μM. **5-AP** was treated to the purified RBCs (8% working concentration, v/v, in cold 1× PBS). [Positive control: 0.1% (working concentration) Triton X-100]. The mixture was incubated in a shaking incubator (200 rpm, 37 °C) for 1 h, followed by centrifugation at 2000 rpm at 4 °C. Hemolysis was assessed by measuring the absorbance of the supernatant at 450 nm.

In vivo toxicity analysis

7-Week-old female ICR mice were randomly divided into three groups (n = 3 per group) as follows: (i) control group (treated with PBS), (ii) positive control group (treated with 25% (v/v) eugenol), and (iii) **5-AP** group (treated with **5-AP**). The mice were then administered PBS (pH 7.4), eugenol, and **5-AP** to the back (250 μM, 50 μL per day) for one week. The body weight and food/water intake were recorded on days 1, 4, and 7. After sacrifice, auricular lymph nodes and blood samples were collected. For analysis of serum histamine and immunoglobulin E levels, blood samples were drawn and allowed to clot for 2 h at 25 °C in a serum separator tube. The clotted samples were then centrifuged (3000 rpm, 15 min). Serum histamine and immunoglobulin E levels were analyzed after the reagent treatment according to the manufacturer's instructions.

Melanoma xenograft mice

B16F10 cells (1×10^6 cells, suspended in 100 μL of a 1:1 mixture of DMEM medium and Matrigel) were subcutaneously injected into the left or right thigh of each mouse. The therapeutic efficacy on mouse tumors was evaluated 7 days after the injection, based on findings from a previous pilot test that confirmed melanoma tumor detection using **5-AP** was possible from day 7.

In vivo photodynamic treatment

After 7 days of melanoma xenograft, PBS, 5-ALA, and **5-AP** were treated transdermal every 2 days for 10 days, and the Laser group was treated with a 530 nm (50 mW cm^{-2}) laser for 3 min, 3 h after PBS, 5-ALA or **5-AP** (250 μM, 50 μL) treatment. After all experiments, perfusion and fixation processes were performed, and then organs including tumor tissues were harvested.

FTIS mouse tissue imaging

After treatment of **5-AP** (25 and 50 μL) on the tumor site, the tumor tissue was dissected for ex vivo analysis. Fluorescence tissue imaging was performed using a fluorescence tissue imaging system (FTIS, VISQUE InVivo Elite, Vieworks Co. Ltd, Rep. of Korea). The imaging experiments were carried out in a dark room. Data were acquired by tracking the fluorescence signals of **5-AP** (Cy5.5 Channel: 390–490 nm excitation, 690–740 nm detection channel).

Hematoxylin & eosin (H&E) staining

Tumor tissues were fixed in 10% buffered formalin (HT501640-19L, Sigma), embedded in paraffin, and sectioned into 6-μm sliced. Then, the tumor sections were stained with H&E. The stained sections were observed under a regular light microscope to determine tumor cell death, growth, and hemorrhage.

Immunohistochemistry (IHC) staining

Tumor tissues were processed into frozen blocks using OCT solution. After freezing, the tissues were sectioned into 6-μm slices. Each section was blocked with 7% horse serum (Gibco) for 30 min, then was incubated with primary antibodies against Ki67 (ab16667, Abcam) or cleaved-caspase 3 (#9661S, Cell Signaling Technology) overnight at 4 °C. The following day, the sections were incubated with a biotin-labeled secondary antibody for 1 h at room temperature, then with the VECTAS-TAIN Elite ABC universal kit and DAB substrate kit, peroxidase with nickel (SK-4100, VECTOR) for detection. Observation and image capture was done using a Evos m7000 (Invitrogen). Average optical density (AOD) was quantified using ImageJ software. The AOD was calculated based on the following formula:

$$AOD = -\log_{10} \frac{\text{Mean Gray Value}}{\text{Max Gray Value}}$$

Statistical analysis

The results were analyzed using ANOVA with Tukey's multiple comparison test. All statistical analyses were performed using Prism 8.0 software (GraphPad, La Jolla, CA, USA).

Results and discussion

Materials preparation and characterization

The 5-aminolevulinic acid (5-ALA) polymer (**5-AP**), based on the ring-opening polymerization of cyclic silanes, was synthesized through an in situ one-pot method under an argon atmosphere. To characterize **5-AP** after its formation, various in vitro analyses were conducted, including gel permeation chromatography (GPC), ^{1}H NMR, attenuated total reflectance Fourier-transform infrared spectrum (ATR-FTIR) spectroscopy, water contact angle measurement, viscosity testing, and thermogravimetric analysis (TGA) (Fig. 2). In the GPC analysis, the molecular weight of **5-AP** was found to be 9878 g mol^{-1}, while the molecular weight of TDOP, a cyclic silane monomer, was found to be 186 g mol^{-1} (Fig. 2(a)). These results demonstrated that **5-AP** was formed as a polymer through the ring-opening polymerization of cyclic silane. ^{1}H NMR was utilized to confirm the ring-opening polymerization process of TDOP with 5-ALA and MeOH as initiators (Fig. 2(b)). ^{1}H NMR was recorded in CDCl$_3$ (7.26 ppm), confirming that the final compound, **5-AP**, consisted of a mixture of 5-ALA-initiated and MeOH-initiated polymers. To conduct an additional qualitative analysis of **5-AP**, ATR-FTIR spectroscopy was performed (Fig. 2(c)). In the ATR-FTIR
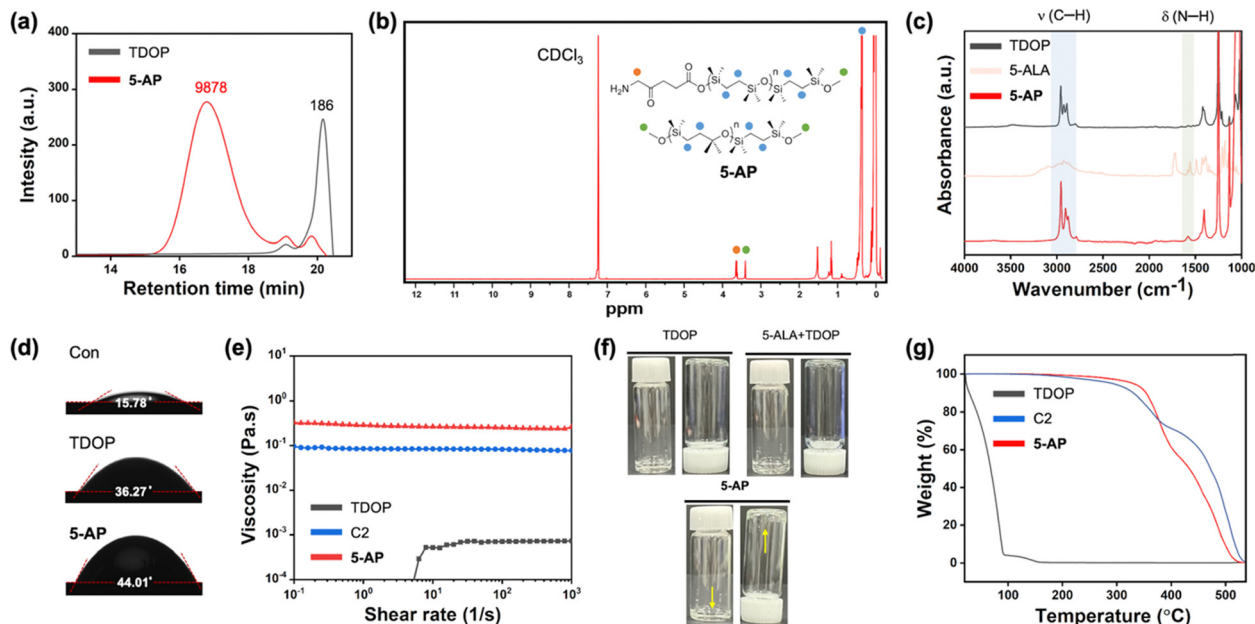
Fig. 2 Characterization of **5-AP**. (a) Gel-permeation chromatography (GPC) analysis spectrum of TDOP (monomer) and **5-AP**. (b) ^{1}H NMR analysis of **5-AP** in CDCl$_3$. (c) Attenuated total reflectance Fourier-transform infrared (ATR–FTIR) spectra of TDOP, 5-ALA, and **5-AP**. Symbols: ν = stretching, δ = bending. (d) Water droplet images on slide glass coated with TDOP and **5-AP**. Inserted numbers indicate the water contact angles on slide glass coated with each sample. (e) Viscosity as a function of shear rate for TDOP, C2, and **5-AP** at 25 °C. (f) Photographs of TDOP, 5-ALA + TDOP, and **5-AP**. (g) Thermogravimetric analysis (TGA) profiles of TDOP, C2, and **5-AP** under a nitrogen atmosphere.

analysis, the ν (C–H) peak of TDOP at 2800–3000 cm^{-1} and the δ(N–H) peak of 5-ALA at 1580–1650 cm^{-1} remained intact in **5-AP**.[39–41] These results indicate that both MeOH-initiated and 5-ALA-initiated polymers exist in **5-AP**, suggesting the possible presence of residual 5-ALA. After the qualitative analysis of **5-AP**, we confirmed its characteristics as a polymer. In the water contact angle measurement, the water contact angle of TDOP in its monomer state was 36.27°, whereas **5-AP**, after polymerization, showed a higher water contact angle of 44.01° (Fig. 2(d)). In addition, the viscosity analysis results revealed that **5-AP** has a higher viscosity than both the monomeric form TDOP and the C2 polymer, which was developed in previous research using citric acid as an initiator (Fig. 2(e)).[42] The results from the water contact angle and viscosity analyses confirmed that **5-AP** is a polymer with significant viscosity, a finding that was also visually confirmed. The photos illustrate that while the TDOP and 5-ALA + TDOP groups settled at the bottom of the vial due to gravity immediately after it was inverted, **5-AP** remained adhered to the top, even when the vial was turned over, indicating its high viscosity (Fig. 2(f)). Lastly, TGA analysis was performed to assess the thermal stability of the polymer, which is known to be relatively high (Fig. 2(g)). As expected, the TGA results demonstrated that **5-AP** exhibits significant thermal stability. Through various *in vitro* assays, we confirmed that **5-AP** was synthesized as a polymer formulation through the ring-opening polymerization of cyclic silanes, using 5-ALA and MeOH as initiators, and that it is both heat-stable and highly viscous. Next, we obtained the time-dependent 5-ALA release profile by hydrolysis of **5-AP** and confirmed that 90% of 5-ALA was released over 10 h (Fig. S1, ESI†). Most of

the treated **5-AP** were observed through the skin within 1 h, so the release of 5-ALA occurred in the tumor site, not the skin surface. We also considered the viscosity change of **5-AP** on the mouse skin surface. As a result, the significant viscosity changes of **5-AP** were not observed in the temperature range of 30–40 °C.

In vitro analysis of 5-AP

After analyzing the characterization of **5-AP** through various *in vitro* assays, we confirmed its efficacy at the cellular level (Fig. 3 and Fig. S2–S4, ESI†). Before analyzing the *in vitro* PDT efficacy of **5-AP** as a photosensitizer, cytotoxicity of **5-AP** was assessed in HEK293, b.End3, and B16F10 cell lines, with and without laser irradiation (Fig. 3(a) and Fig. S2, ESI†). The results revealed that **5-AP** displayed minimal toxicity in HEK293 and b.End3 cell lines. However, in the B16F10 cell line, **5-AP** displayed a tendency for toxicity even in the absence of laser irradiation and caused significantly higher cytotoxicity when irradiated with a 530 nm laser. In contrast, TDOP and 5-ALA did not exhibit any toxicity in HEK293, b.End3, and B16F10 cell lines (Fig. S3, ESI†). These cytotoxicity results suggest that 5-ALA can be released from **5-AP** through degradation in biological media and subsequently converted into PpIX *via* heme synthesis in B16F10 tumor cells.[42] To visually confirm this conversion process from 5-ALA to PpIX, we obtained confocal fluorescence images of HEK293, b.End3, and B16F10 cell lines (Fig. 3(b) and Fig. S4, ESI†). The images showed no emission in HEK293 and b.End3 cell lines were treated with **5-AP**, but notable PpIX emission was observed in the B16F10 cell line. These results confirm that 5-ALA is released from **5-AP** and
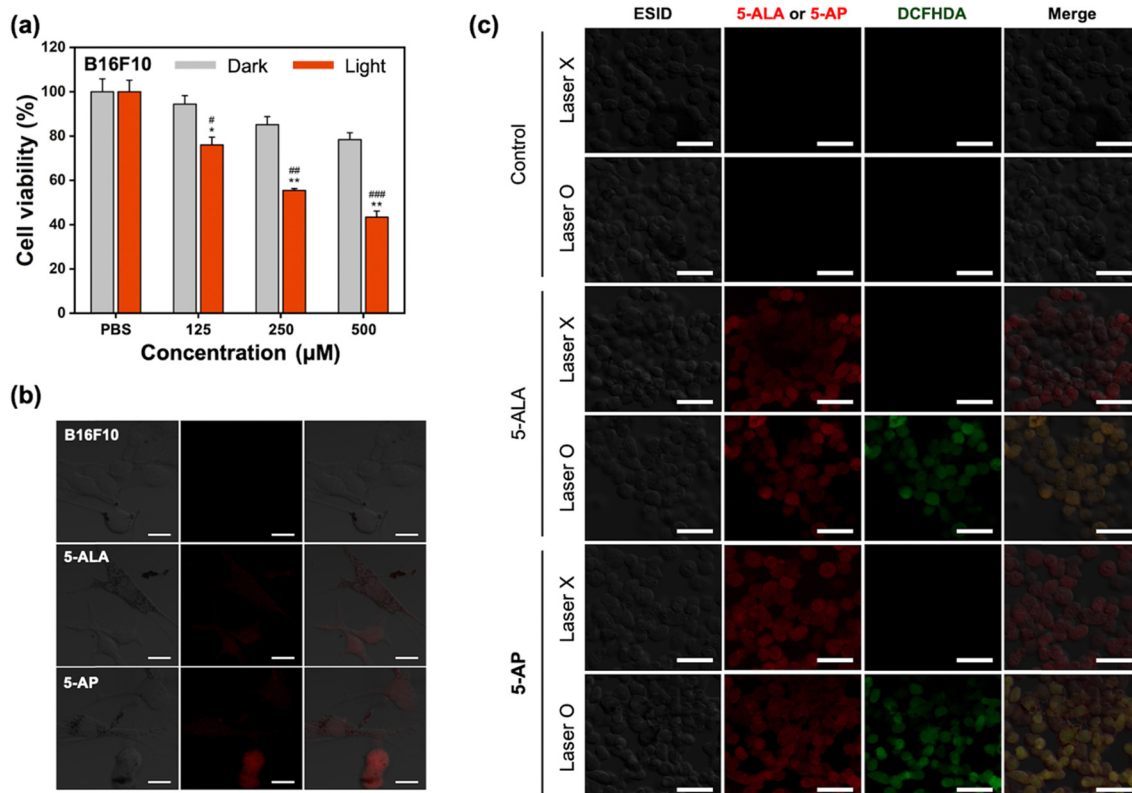
Fig. 3 Cytotoxicity assay and cellular imaging. (a) Cell viability results of **5-AP** in B16F10 cells with/without laser irradiation (530 nm) using a CCK-8 assay kit. Incubation time: 4 h (37 °C), irradiation time: 2 min. Data are presented as the mean ± S.E.M. ($n = 3$). $*p < 0.05$, $**p < 0.01$ compared to the PBS group; $\#p < 0.05$, $\#\#p < 0.01$, $\#\#\#p < 0.005$ compared to the dark group at the same concentration. (b) Confocal laser scanning microscopy (CLSM) images of B16F10 cells after treatment with 5-ALA and **5-AP** (concentration: 250 μM). Incubation time: 2 h (37 °C). Scale bar: 20 μm. (c) The *in vitro* ROS generation of 5-ALA and **5-AP** (concentration: 250 μM) against B16F10 cells with/without laser irradiation (530 nm). Scale bar: 40 μm. Confocal images were obtained under excitation at 488 nm (laser power: 0.23%) using a detector (GaAsP, detector gain: 700 V; detector wavelength: 504–700 nm).

successfully converts to PpIX in the melanoma cancer cell line. Next, confocal fluorescence imaging of cells using DCFHDA, a fluorescent probe that can sense reactive oxygen species (ROS), was conducted to identify the ROS-mediated tumor cell killing mechanism during laser irradiation. As a result, we confirmed that ROS was equally generated from both 5-ALA and **5-AP** when irradiated with laser, and together with the previous results, we proved that **5-AP** is converted to PpIX inside tumor cells and generates ROS (Fig. 3(c)).

In vivo toxicity analysis of 5-AP

After confirming the cellular PpIX generation from **5-AP** and the photo-induced therapeutic results, we conducted the *in vivo* toxicity analysis of **5-AP** (Fig. 4). First, a hemolysis assay was performed to determine the working concentration of the substance in an *in vivo* assay (Fig. 4(a)). The group treated with Triton X-100 demonstrated hemolytic activity, whereas **5-AP** did not show any hemolytic activity within the concentration range of 125 to 500 μM. Based on these results, the concentration of **5-AP** for the *in vivo* toxicity analysis was set at 250 μM (50 μL), and **5-AP** was applied to the back skin of the mice daily for 7 days. Eugenol (Eug), a known immunotoxicity agent, was used as a positive control to assess immunotoxicity. The toxicity

evaluation of **5-AP** included monitoring changes in body weight, food and water intake, lymph node weight, histamine levels, and immunoglobulin E (IgE) levels. There were no significant differences in body weight changes between the **5-AP**-treated group and the normal group treated with phosphate-buffered saline (PBS, pH 7.4) on both day 1 and 7 (Fig. 4(b)). Similarly, food and water intake showed no notable differences between the **5-AP**-treated group and the other groups on both days 1–4 and 5–7 (Fig. 4(c)). In contrast, the weight of lymph nodes—the key indicator for assessing immunotoxicity—showed substantial enlargement in the Eug-treated group compared to both the PBS-treated and **5-AP**-treated groups (Fig. 4(d)). However, there were no considerable differences between PBS treated group and the **5-AP**-treated group. The serum histamine level greatly increased in the group treated with Eug (Fig. 4(e)). In the **5-AP**-treated group, the histamine level was slightly elevated compared to the PBS-treated group, but this difference was not statistically significant. A similar pattern was confirmed in the IgE levels mirroring the lymph node weight results (Fig. 4(f)). In the Eug-treated group, the IgE level markedly increased compared to both the PBS-treated and **5-AP**-treated groups. However, no meaningful differences were observed between the **5-AP**-treated and the
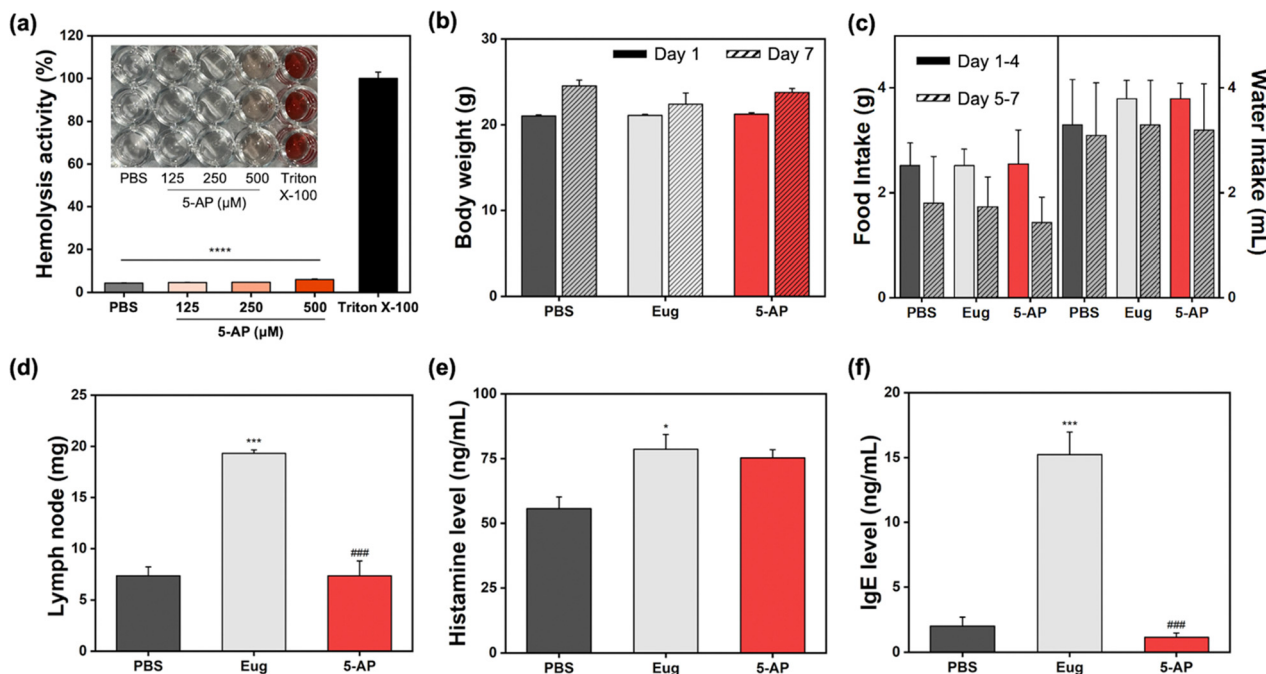
Fig. 4 *In vivo* toxicity data of **5-AP**. (a) Hemolysis analysis results of **5-AP**. Data are presented as the mean ± S.E.M. ($n = 3$). **** < 0.001 compared to the Triton X-100 group. (b) Weight change on the first and last days during the 7-day administration of Eug (eugenol) and **5-AP** (250 μM, 50 μL per day). Data are presented as the mean ± S.E.M. ($n = 3$). (c) Food and water intake for days 1–4 and 5–7. Data are presented as the mean ± S.E.M. ($n = 3$). (d) Lymph node weight after 7 days of Eug (eugenol) and **5-AP** treatment. Data are presented as the mean ± S.E.M. ($n = 3$). ***$p < 0.005$ compared to the PBS group; ###$p < 0.005$ compared to the Eug group. (e) Serum histamine levels (unit: ng mL^{-1}) and (f) serum immunoglobulin E levels (unit: ng mL^{-1}) in the blood of mice in each group. Data are presented as the mean ± S.E.M. ($n = 3$). *$p < 0.05$, ***$p < 0.005$ compared to the PBS group; ###$p < 0.005$ compared to the Eug group.

PBS-treated groups. These *in vivo* toxicity results suggest that while **5-AP**, an external substance, induced a slight increase in histamine levels, it did not cause overall immunotoxicity. This confirms its suitability for use as a photosensitizer *in vivo*.

In vivo therapeutic efficacy analysis of 5-AP

Based on the *in vivo* toxicity assay results, we performed an *in vivo* therapeutic efficacy analysis of **5-AP** as a photodynamic therapy agent in a melanoma mouse model (Fig. 5). A melanoma mouse model was prepared by xenografting B16F10 cells into the thighs of BALB/c nu/nu mice, followed by the administration of **5-AP** with laser irradiation (Fig. 5(a)). Before verifying the efficacy of PDT, we aimed to determine the appropriate dose of **5-AP** and the timing of conversion of **5-AP** to PpIX in melanoma tumors. To this end, we first treated mice with different doses of **5-AP** and examined the fluorescence changes over time (Fig. 5(b) and (c)). As a result, it was confirmed that **5-AP** has high radiant efficiency over time in a concentration-dependent manner. To verify the improved bioavailability of **5-AP** compared to 5-ALA, we measured the fluorescence intensity in the tumor area over time after treatment of 5-ALA (i.p., topical) and **5-AP** (topical) (Fig. S5, ESI†). As a result, the **5-AP**-treated set (at the same concentration as 5-ALA) gave a higher signal compared with the 5-ALA-injected set and 5-ALA-topical set. These results demonstrate that **5-AP** has higher bioavailability in tumors than conventional 5-ALA treatment methods. Given this rapid PpIX conversion and the mice's recovery, PDT

using **5-AP** and laser (530 nm) was initiated 7 days after the B16F10 xenograft. PDT was then performed at 2-day intervals for 10 days (Fig. 5(a)). As this mouse model was xenografted with B16F10 cells on the thigh, there was no significant change in body weight over the 10 days (Fig. 5(d)). Non-significant changes in body weight were also observed in the laser irradiation and 5-ALA or **5-AP** treatment sets. In contrast, tumor size showed a clear difference between each group over time (Fig. 5(e)). Compared to the group treated with PBS alone, the groups treated with 5-ALA or **5-AP** followed by laser showed a significant tumor reduction effect. This difference was even greater in the **5-AP** + Laser group, and a significant tumor size reduction was confirmed when compared to the 5-ALA + Laser group. These differences were clearly visible in the macroscopic tumor observations of mice on day 10, and the same pattern was observed in the harvested tumors (Fig. 5(f) and (g)). We also confirmed that a marked increase in radiant efficiency was observed in the harvested tumors, while no fluorescence change was observed in other organs (brain, heart, lung, spleen, kidney, liver) (Fig. S6, ESI†). The results indicated that the **5-AP** could minimize drug-induced side effects due to the localized PpIX generation at the tumor site. To further confirm that these results were not due to the photothermal effect, we conducted a thermal imaging analysis to examine the changes in body temperature after treatment of 5-ALA and **5-AP** with a laser (Fig. S7, ESI†). As a results, the body temperatures were similar in all mouse groups, and these results indicated that
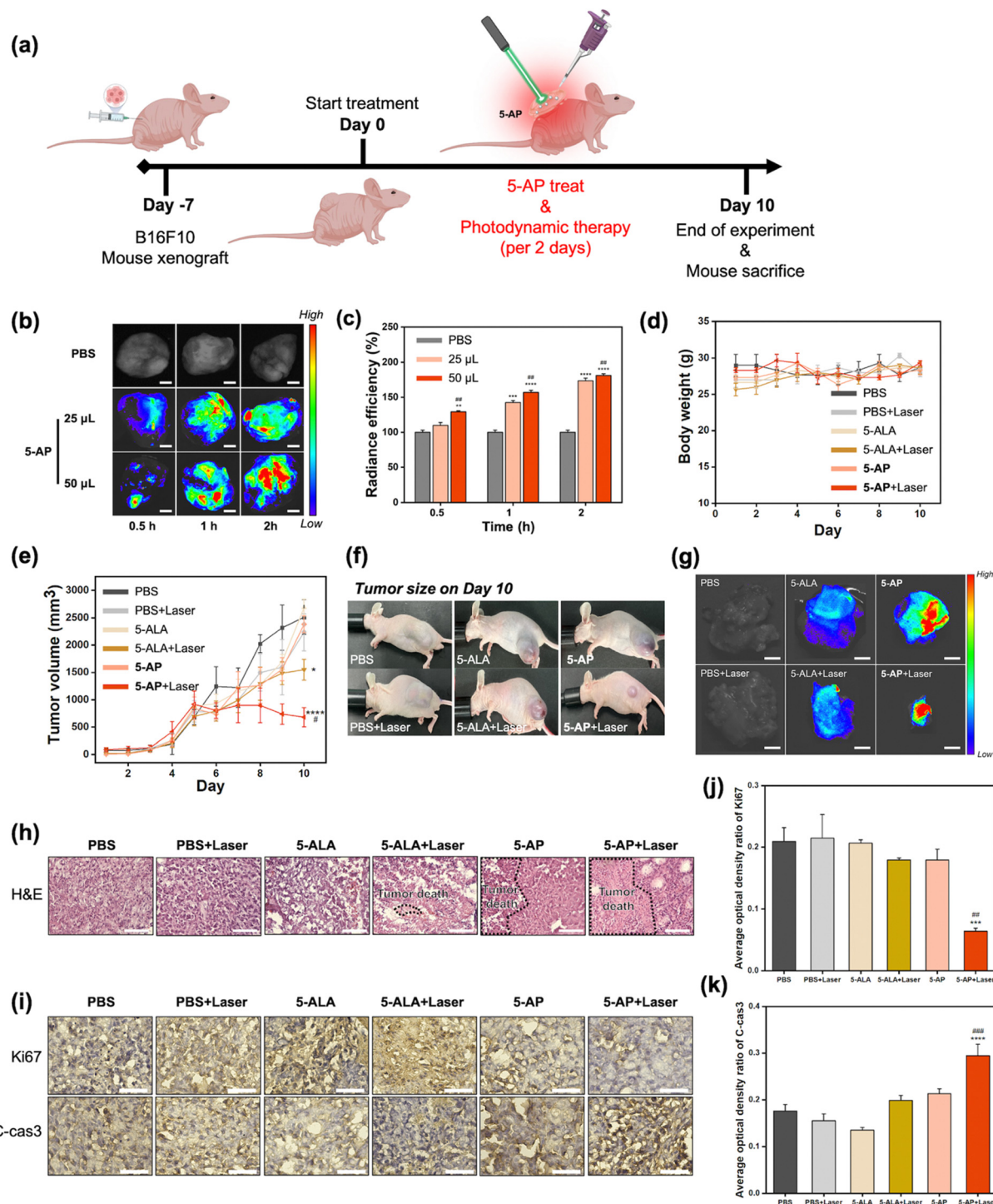
Fig. 5 *In vivo* therapeutic efficacy of **5-AP**. (a) Schematic illustration of the *in vivo* experiment. (b) Fluorescence images of the melanoma tumor site using FITS after **5-AP** treatment on day 0. The times (0.5, 1, 2 h) indicate the time elapsed after **5-AP** (250 μM, 50 μL per day) application. Scale bar: 5 mm. (c) Radiant efficiency of each mouse from the FTIS image. Data were acquired by tracking the signals of **5-AP** (Cy5.5 Channel: 390−490 nm excitation, 690−740 nm detection channel). Data are presented as the mean ± S.E.M. (n = 3). ** < 0.01, *** < 0.005, **** < 0.001 compared to the PBS group; ##p < 0.01 compared to the 25 μL **5-AP** treated group. (d) Changes in body weight from day 1 to 10. (e) Changes in tumor volume from day 1 to 10. Data are presented as the mean ± S.E.M. (n = 3). * < 0.05, **** < 0.001 compared to the PBS group; #p < 0.05 compared to the 5-ALA + Laser group. The laser was used a 530 nm wavelength laser. (f) Photographs of melanoma xenograft mice on day 10. (g) Fluorescence images of the harvested melanoma tumor using FITS on day 10. Scale bar: 10 mm. (h) Representative H&E staining results of the melanoma tumor in each group. Scale bar: 75 μm. (i) Representative photomicrographs Ki67 and cleaved caspase 3 (C-cas3) immunostaining in the melanoma tumor of each group. Scale bar: 50 μm. (j), (k) Average optical density of (j) Ki-67 and (k) C-cas3 staining evaluated by Image J software. Data are presented as the mean ± S.E.M. (n = 3). *** < 0.005, **** < 0.001 compared to the PBS group; ##p < 0.01, ### < 0.005 compared to the 5-ALA + Laser group.

the melanoma therapeutic character of **5-AP** was derived from PDT effect. Finally, the therapeutic efficacy of **5-AP** against melanoma was verified through histological analysis (Fig. 5(h)–(k)). We analyzed the histopathological alteration in melanoma tissues by hematoxylin and eosin (H&E) staining. The PBS + Laser control group showed similar results to the PBS group, indicating that the laser alone did not affect the tumor growth. The **5-AP** + Laser-treated group exhibited the most extensive necrotic lesions (Fig. 5(h)). Further IHC staining was done to determine pathways related to the proliferation and apoptosis of melanoma. The **5-AP** + Laser group demonstrated suppressed Ki67 expression, indicating reduced tumor cell proliferation.[43] Additionally, **5-AP** + Laser treatment increased cleaved-caspase 3 expression, suggesting an activation of the apoptotic program.[44] These results demonstrate that nearly all melanomas were apoptotic following 10 days of **5-AP** PDT. Analysis of the *in vivo* therapeutic effect of **5-AP** confirms that **5-AP** can act as an effective PDT agent with transdermal delivery ability.

Conclusions

We disclose a new 5-ALA-based polymer, named **5-AP**, through the ring-opening polymerization of cyclic silane to overcome the low transdermal absorption rate of 5-ALA for melanoma treatment. The preparation and characterization of **5-AP** were systematically conducted through various analytical methods. Cell-based experiments verified that **5-AP** retains the characteristics of existing 5-ALA, converts to PpIX, emits fluorescence, and maintains its PDT efficacy. In melanoma xenograft animal experiments, **5-AP** demonstrated suitable safety for *in vivo* use and induced melanoma tumor elimination in a short period through its high PDT efficacy. We are confident that **5-AP** is a promising new PDT agent capable of transdermal delivery, and our rationale can usher in new research in melanoma treatment.

Author contributions

Jaehoon Kim: conceptualization, methodology, investigation, visualization, writing – original draft, writing – review & editing. Eun Woo Seo: methodology, investigation, visualization. Hyunyoung Choi: methodology. Hyo In Kim: methodology. Jinbong Park: methodology. Junyang Jung: supervision, project administration. Dokyoung Kim: conceptualization, funding acquisition, project administration, supervision, writing – review & editing.

Data availability

The data that support the findings of this study are available from the corresponding author, D. Kim, upon reasonable request.

Conflicts of interest

The authors declare the following competing financial interest(s): the authors are listed as inventors on a pending patent application related to the technology described in this work.

References

1 Y. Feng, G. Wang, W. Li, J. Yan, X. Yu, H. Tian, B. Li and Y. Dai, *Adv. Healthcare Mater.*, 2024, **13**, 2302811.

2 A. J. Miller and M. C. Mihm Jr, *N. Engl. J. Med.*, 2006, **355**, 51–65.

3 D. Schadendorf, A. C. Van Akkooi, C. Berking, K. G. Griewank, R. Gutzmer, A. Hauschild, A. Stang, A. Roesch and S. Ugurel, *Lancet*, 2018, **392**, 971–984.

4 D. Schadendorf, D. E. Fisher, C. Garbe, J. E. Gershenwald, J.-J. Grob, A. Halpern, M. Herlyn, M. A. Marchetti, G. McArthur and A. Ribas, *Nat. Rev. Dis. Primers*, 2015, **1**, 1–20.

5 J.-C. Martinez and C. C. Otley, *Mayo Clin. Proc.*, 2001, **76**(12), 1253–1265.

6 J. Chen, H. Niu, L. Guan, Z. Yang, Y. He, J. Zhao, C. Wu, Y. Wang, K. Lin and Y. Zhu, *Adv. Healthcare Mater.*, 2023, **12**, 2202474.

7 S. Bhatia, S. S. Tykodi and J. A. Thompson, *Oncology*, 2009, **23**, 488.

8 Q. Liu, M. Das, Y. Liu and L. Huang, *Adv. Drug Delivery Rev.*, 2018, **127**, 208–221.

9 K. T. Flaherty, J. R. Infante, A. Daud, R. Gonzalez, R. F. Kefford, J. Sosman, O. Hamid, L. Schuchter, J. Cebon and N. Ibrahim, *N. Engl. J. Med.*, 2012, **367**, 1694–1703.

10 V. Subbiah, C. Baik and J. M. Kirkwood, *Trends Cancer*, 2020, **6**, 797–810.

11 F. Meric-Bernstam and G. B. Mills, *Nat. Rev. Clin. Oncol.*, 2012, **9**, 542–548.

12 L. Zhong, Y. Li, L. Xiong, W. Wang, M. Wu, T. Yuan, W. Yang, C. Tian, Z. Miao and T. Wang, *Signal Transduction Targeted Ther.*, 2021, **6**, 1–48.

13 S. V. Sheleg, E. A. Zhavrid, T. V. Khodina, G. A. Kochubeev, Y. P. Istomin, V. N. Chalov and I. N. Zhuravkin, *Photodermatol., Photoimmunol. Photomed.*, 2004, **20**, 21–26.

14 L. M. Lifshits, J. A. Roque III, P. Konda, S. Monro, H. D. Cole, D. von Dohlen, S. Kim, G. Deep, R. P. Thummel and C. G. Cameron, *Chem. Sci.*, 2020, **11**, 11740–11762.

15 J. Kim, E. W. Seo, J. Lee, J. Lee, M. Jeong, H. Jeong and D. Kim, *Coord. Chem. Rev.*, 2024, **502**, 215624.

16 J. Kim, J. H. Kim, E. W. Seo, Y. Kim, J. Kang, C. W. Koh, I. G. Ju, H. Eo, S. Park, M. S. Oh and D. Kim, *Chem. Eng. J.*, 2024, **479**, 147703.

17 Y.-Y. Huang, D. Vecchio, P. Avci, R. Yin, M. Garcia-Diaz and M. R. Hamblin, *Biol. Chem.*, 2013, **394**, 239–250.

18 L. Davids and B. Kleemann, *Cancer Treat. Rev.*, 2011, **37**, 465–475.

19 A. Kawczyk-Krupka, A. M. Bugaj, W. Latos, K. Zaremba and A. Sieroń, *Photodiagn. Photodyn. Ther.*, 2013, **10**, 503–509.

20 J. Hu, Y. a Tang, A. H. Elmenoufy, H. Xu, Z. Cheng and X. Yang, *Small*, 2015, **11**, 5860–5887.

21 W. Fan, P. Huang and X. Chen, *Chem. Soc. Rev.*, 2016, **45**, 6488–6519.

22 J. C. Kennedy, S. L. Marcus and R. H. Pottier, *J. Clin. Laser Med. Sur.*, 1996, **14**, 289–304.

23 Q. Peng, T. Warloe, K. Berg, J. Moan, M. Kongshaug, K. E. Giercksky and J. M. Nesland, *Cancer*, 1997, **79**, 2282–2308.

24 S. Sansaloni-Pastor and N. Lange, *J. Photochem. Photobiol., B*, 2023, **247**, 112771.

25 Z. Malik, *Transl. Biophotonics*, 2020, **2**, e201900022.

26 R. F. V. Lopez, N. Lange, R. Guy and M. V. L. B. Bentley, *Adv. Drug Delivery Rev.*, 2004, **56**, 77–94.

27 M. B. R. Pierre, E. Ricci, A. C. Tedesco and M. V. L. B. Bentley, *Pharm. Res.*, 2006, **23**, 360–366.

28 A. A. Seetharam, H. Choudhry, M. A. Bakhrebah, W. H. Abdulaal, M. S. Gupta, S. M. D. Rizvi, Q. Alam, Q. A. Siddaramaiah, D. V. Gowda and A. Moin, *Pharmaceutics*, 2020, **12**, 1101.

29 M. R. Prausnitz and R. Langer, *Nat. Biotechnol.*, 2008, **26**, 1261–1268.

30 W. Y. Jeong, M. Kwon, H. E. Choi and K. S. Kim, *Biomater. Res.*, 2021, **25**, 24.

31 A. M. Wokovich, S. Prodduturi, W. H. Doub, A. S. Hussain and L. F. Buhse, *Eur. J. Pharm. Biopharm.*, 2006, **64**, 1–8.

32 V. Phatale, K. K. Vaiphei, S. Jha, D. Patil, M. Agrawal and A. Alexander, *J. Controlled Release*, 2022, **351**, 361–380.

33 R. Neupane, S. H. Boddu, M. S. Abou-Dahech, R. D. Bachu, D. Terrero, R. J. Babu and A. K. Tiwari, *Pharmaceutics*, 2021, **13**, 960.

34 V. Krishnan and S. Mitragotri, *Adv. Drug Delivery Rev.*, 2020, **153**, 87–108.

35 N. Dragicevic, J. Predic-Atkinson, B. Nikolic, S. B. Pajovic, S. Ivkovic and M. Adzic, *Expert Opin. Drug Delivery*, 2024, **21**, 279–307.

36 N. Gupta, G. Gupta and D. Singh, *Front. Nanotechnol.*, 2022, **4**, 1006628.

37 F. S. G. Praça, P. M. Campos, J. O. Eloy, R. Petrilli, M. V. L. B. Bentley and W. S. G. Medina, *Carrier-Mediated Dermal Delivery*, Jenny Stanford Publishing, 2017, pp. 123–172.

38 W. Zhan, H. Yi, S. Song, Y. Zhao and F. Rao, *Colloids Surf., A*, 2019, **568**, 36–42.

39 M. A. R. George and O. Dopfer, *Phys. Chem. Chem. Phys.*, 2023, **25**, 5529–5549.

40 A. Krüger, A. Bürkle, A. Mangerich and K. Hauser, *Biomed. Spectrosc. Imaging*, 2018, **7**, 25–33.

41 W. Witoonsaridsilp, O. Paeratakul, B. Panyarachun and N. Sarisuta, *AAPS PharmSciTech*, 2012, **13**, 699–706.

42 H. Um, R. H. Kang, J. Kim, E. W. Seo, J. Ahn, J. Lee and D. Kim, *Polymer*, 2023, **283**, 126271.

43 P. Quatresooz and G. E. Piérard, *Am. J. Clin. Dermatol.*, 2011, **12**, 77–86.

44 S. Fulda, *Semin. Cancer Biol.*, 2015, **31**, 84–88.